Journal of Neonatal Surgery
ISSN(Online): 2226-0439
Vol. 14,issue.33s (2025)
https://www.jneonatalsurg.com

OPEN ACCESS

A Reread Deep Neural Network for Multiclass Lung Disease Detection and Classification

N. Suganthi[1], Dr.K.Sarojini [2]

[1]Research Scholar, PG and Reasearch Department Of Computer Science Chikkanna Government Arts College,Tirupur
Email ID : suganca@gmail.Com

[2]Assistant ProfessorPG and Research Department Of Computer Science, Chikkanna Government Arts College,Tirupur
Email ID : saromaran@gmail.Com

Cite this paper as N. Suganthi, Dr.K.Sarojini .(2025) A Reread Deep Neural Network for Multiclass Lung Disease Detection and Classification . .Journal of Neonatal Surgery, 14, (33s), 114-134

ABSTRACT

COVID-19 is a dangerous and extremely infectious virus, destroyed the life of million people throughout the world. Early viral identification can lower virus propagation and mortality rates. A number of different detection techniques have been implemented to identify COVID-19 in Computed Tomography (CT) scans. Amongst, Chaotic Logistic Map based Modified Whale Optimization with Improved Neural Network (CLM-MWO-INN) provides an efficient result in COVID-19 prediction. However, it cannot process large size samples. Hence, in this paper, a Reread Deep Neural Network (RDNN) model is proposed for processing the large number of samples from CT images. Gray Level Run Length Matrix (GLRLM) and Gray Level Co-Occurrence Matrix (GLCM) is used to produce the handmade features, whereas RDNN's convolutional layers are used to extract the deep features. These extracted attributes are combined and appropriate features are selected by CLM-MWO. The CLM-MWO is also used for selecting an appropriate parameter of RDNN.The feature and parameter selection are simultaneously performed in this model, because the selected features and parameter might affect the RDNN performance. The selected features by CLM-MWO are fed into the softmax layer classifies CT lung scan images into multiple classes, including Atelectasis, Pneumonia, Infiltrate, COVID-19, and Non-Diseased. The suggested approach yields favorable outcomes when compared to traditional DNN architectures, exhibiting improved convergence speed with larger datasets. The complete work is named as CLM-MWO with RDNN (CLM-MWO-RDNN). At last, the results show that compared to state-of-the-art models, the CLM-MWO-RDNN model outperforms with an accuracy of 98.59% (single validation) and 97.28% (4-fold cross validation) on the SARS-CoV-2 CT scan dataset, 97.74% (without augmentation) and 96.32% (with augmentation and 4-fold cross validation) on Customized Lung disease dataset than ViT- LSTM and ViT-CNN-LSTM models.

Keywords: *COVID-19, Reread Deep Neural Network, hand-crafted features, deep features, Computed Tomography Images.*

1. INTRODUCTION

SARS-CoV-2 causes the coronavirus sickness known as COVID-19. The virus was formally called COVID-19 by the World Health Organization (WHO) on February 11, 2020 (WHO, 2020). [1]. By June 2021, approximately 180 million confirmed cases had been reported, according to data gathered by the WHO, as the virus rapidly spread beyond its initial point of origin [2].

COVID-19 screening begins at primary care or hospitals, with imaging used for rapid assessment while Reverse Transcription-Polymerase Chain Reaction (RT-PCR) remains the standard technique for prediction [3]. Then, patients with severe respiratory symptoms undergo chest X-rays (CXR) and CT scans if more detail is required. Imaging techniques are fast and practical, helping clinicians quickly identify the disease and assess its severity. As a result, CXR and CT scans are widely adopted as alternative diagnostic tools in clinical settings [4].

To improve diagnosis, doctors examine CXR/CT images of the lungs to identify signs of COVID-19- related changes. Patient cases have increased significantly due to the rapid dissemination of COVID-19, making the process of assessing the virus's progression both labor-intensive and time-consuming. This challenge can be addressed by leveraging Machine Learning (ML) methods for more efficient detection of COVID-19. Medical imaging with Computer-Aided Diagnosis (CAD) has made significant use of ML approaches in recent years, with the goal of boosting up the process of detecting COVID-19 patients. [5]

For instance, a ML-based system has been developed to identify COVID-19 from CT/CXR images [6]. The images were pre-processed with fuzzy c-means (FCM) clustering for normalization and segmentation which extracts statistical, textural and Wavelet Transform (WT) features. using Principal Component Analysis (PCA) was used to select relevant features. K-

Nearest Neighbour, Artificial Neural Networks (ANN) and Support Vector Machines (SVM) was applied to classify normal, pneumonia or COVID-19 This model aims for early detection, but classifier performance depends on predefined parameters. Also, hyper-parameter regularization enhances the network generalization across different datasets

To choose an appropriate hyper parameters and feature selection for effectively improving performance of classifier, CLM-MWO-INN was developed [7]. The CLM-MWO-INN framework is divided into two parts. Using the GLCM and GLRLM techniques, the attributes are first derived from the CT images. Second, the CLM-MWO algorithm was used to choose an appropriate hyper parameters and feature selection for INN classifier's efficiency. This model simultaneously performs hyperparameter tuning and feature selection due to their independence. But, lower result was obtained on large size sample and identifying the optimal number of nodes in INN structure is another challenging task.

The DNN method effectively addresses the problem by efficiently extracting features from CXR/CT images, minimizing training cycles to differentiate between healthy, pneumonia, and COVID-19 cases. It plays a key role in diagnosing COVID-19 by tackling complex challenges in disease identification [8].

On motivating by this, this paper develops the CLM-MWO-RDNN model to process a large number of samples without affecting COVID-19 classification performance. In order to construct an RDNN model, it is necessary to define parameters like the quantity of layers of convolution, maximum pooling layers, convolution filter sizes, hidden layers, Fully Connected (FC) layer, and the number of nodes in each layer. Additionally, training parameters like the learning rate and regularization methods (e.g., sigmoid and tangent functions) must be defined. In RDNN model, deep features extracted by convolutional layers of RDNN and the handcrafted features extracted by GLCM and GLRLM are combined after FC layer. The handcrafted features combined here with the aim of capturing visual characteristics of an image especially, its texture. To improve training accuracy, the CLM-MWO method is then used to choose the right features and parameters. Feature selection and parameter tuning are conducted simultaneously, as the chosen model features can affect hyperparameter efficiency. The selected features are then inputted into the softmax layer for classification. This proposed method demonstrates improved accuracy and a faster convergence rate compared to traditional DNN methods.

The rest of the paper is structured as, research on COVID-19 prediction is reviewed in Section 2. The suggested study framework is described in Section 3 and its efficacy is shown in Section IV. Section V concludes the study and suggests future directions.

2. LITERATURE SURVEY

A Multi-Class CNN (MC-CNN) structure was presented [9] to classify the lung diseases from CT images. But, the considered database was limited, and the restrictions affect the prediction metrics.

In order to identify COVID-19 instances in CT scans, Deformable ResNet50 model was devised [10]. However, this model results in lower classification accuracy. A COVID-19 recognition model was created [11] using Improved Attention ResNet called COVID-ResNet. However, this model faces difficulty in feature extraction lesions were not addressed properly, which decrease the precision.

To predict the presence of COVID-19 in lung CT scans, a Duffing Equation Tuna Swarm (DETS) Optimized ResNet 101 (DETSOR) classifier was presented [12]. But, this model results in overfitting issues and reduce the classifcation accuracy. In order to classify COVID-19 using CT and X-ray images, Deep Transfer Learning (Deep TL) was devised [13]. ConvNeXt, EfficientNetV2, DenseNet121 and ResNet34 were applied as TL models. Among these models, ConvNeXt provides efficient predict results. However, the models hyper-parameter was not fine-tuned properly lowering the accuracy rate.

To detect COVID-19 in CT scans, Salarabadi et al. HTL-FED model was constructed [14] which combines TL with Fuzzy Edge Detection. But, this model results in uncertainty issues which lowers the models prediction performances. A technique for detecting COVID-19 in chest CT images was created [15] by combining ensemble classification with optimized deep features. VGG19 and ResNet 50 was employed to extract the features., Max voting ensemble classification (MVEC) was used for the COVID19 detection. However, this model results in uncertainty issues which lowers the models performances.

3. PROPOSED METHODOLOGY

This section provides a brief description of the CLM-MWO-RDNN model. Initially, image-processing techniques (GLCM, GLRLM) are applied for extracting handcrafted attributes from the given dataset [7]. The RDNN uses convolutional layers to generate deep features, which are combined with extracted information using CLM-MWO, and then input into softmax layers for Lung disease categorization. Fig. 1 shows a schematic depiction of the study as a whole. Table 1 shows the suggested model's notation list.

Table 1. Notation List

Notations	Description
GLCM and GLRLM	
a, b	Row and column index of gray scale matrix of pixels
$\mathcal{P}(a, b)$	Normalized gray level element at a^{th} row and b^{th} column of gray matrix
μ and σ	Mean and Varaince
N_g	Number of gray level values
N_r	Number of Run Length
Z_{ij}	Element of GLRLM with i^{th} row and j^{th} column of gray matrix
$R_{\max}$	Maximum Run Length
N	Number of total pixels in ROI
ln	Natural logarithmic
Deep Convolutional Layer	
x	Input feature map in convolutional layer
w, b	weight and bias
h	Output feature map generated in the convolution layer
o^l	Output layer
$\times$	Convolutional Operation
k	Convolution kernel
$K^{(l)}$	Convolution kernel
f	pooling Function
f^{max}	Max-pooling Function
o^l	Final Extracted Features from FC layer
n_label	Numerical Quantity in image Label
y_j	Predicted Label
CLM-MWO algorithm	
X_f , X_p	Whale position for selecting features and parameters
$X_f{}^{\times}$, $X_p{}^{\times}$	Best solution for feature and parameter selection
D	Distance between the initial whales position
$\lvert\cdot\rvert$	Absolute value operation
$\bullet$	Element wise Multiplication
l	spiral movement of whale

A	Spiral Position Adjustment Factor
a	Exploitation-Exploration Balance Factor
C	Coefficient Vector for Distance Weighting
t	Number of iteration
r	Random Number
D'	Distance between best whale position
q	Constant Integer
i, l	Indices
$cu^{(f)}$, $cu^{(p)}$	Best Feature and Parameter values selected by whale
μ	Behavioural factor in whale
$F_f(i)$ $F_p(i)$	Fitness function for feature and parameter
ϑ_f , ϑ_p	Whale population for feature and parameter
α_f , α_p	Weighting factor of feature and parameter
n_f , n_p	Total number of features and parameters
g	Highest number of iteration

Extracting handcraft features using GLCM and GLRLM

In this model, GLCM and GLRLM are used to extract handcraft features

GLCM Technique: GLCM is a crucial technique for evaluating image texture attributes by analyzing the probability density of pixel relationships within the image**.** [16]. GLCM features are calculated from normalized gray level elements $\mathcal{P}$ from the pixel matrix of N_g grayscale values with a rows and b columns. Eq. (1) - Eq. (8) are used to compute the following GLCM-derived texture features.

$$Contrast = \sum_{a,b=0}^{N_g-1} \mathcal{P}_{a,b}(a,b)^2 \quad (1)$$

$$Correlation = \sum_{a,b=0}^{N_g-1} \mathcal{P}_{a,b} \left[\frac{(a-\mu_a)(b-\mu_b)}{\sqrt{(\sigma_a^2)(\sigma_b^2)}} \right] \quad (2)$$

$$Mean, \mu_a = \sum_{a,b=0}^{N_g-1} a(\mathcal{P}_{a,b});$$

$$\mu_b = \sum_{a,b=0}^{N_g-1} b(\mathcal{P}_{a,b}) \quad (3)$$

$$Variance, \sigma_a^2 = \sum_{a,b=0}^{N_g-1} \mathcal{P}_{a,b}(a-\mu_a)^2;$$

$$\sigma_b^2 = \sum_{a,b=0}^{N_g-1} \mathcal{P}_{a,b}(b-\mu_b)^2 \quad (4)$$

$$SD\ \sigma_a = \sqrt{\sigma_a^2}; \sigma_b = \sqrt{\sigma_a^2} \quad (5)$$

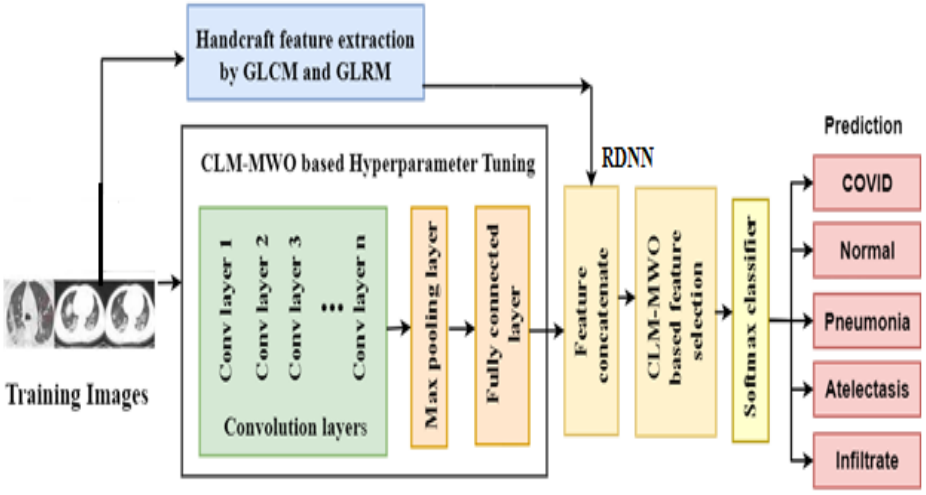

Figure. 1 Working model of the optimized RDNN

$$Entropy = \sum_{a,b=0}^{N_g-1} \mathcal{P}_{a,b}\left(-\ln \mathcal{P}_{a,b}\right) \quad (6)$$

$$Energy = \sum_{a,b=0}^{N_g-1} \mathcal{P}_{a,b}^2 \quad (7)$$

$$Homogeneity = \sum_{a,b=0}^{N_g-1} \frac{\mathcal{P}_{a,b}}{1+(a-b)^2} \quad (8)$$

GLRLM Technique: It is utilized to derive texture features for detailed texture analysis [17]. In GLRLM, Z denotes the GLRLM, Z_{ij} is the $(i,j)^{th}$ entry of the GLRLM. Also, N_r represents the set of different run-length that actually appeared in ROI and N_g defines the set of gray scale images. N denotes the total pixel in the ROI. The N_r systematically searches the image in a specified direction to find sequences of pixels with identical gray levels (N_g). These $N_g - N_r$ features forms a part of statistical features used in texture analysis. The general representation of the run-length matrix in given in Eq. (9)

$$R\,(i,j) = (g\,(i,j) \mid i), 0 \le i \le N_g\,, 0 \le j \le R_{max}\,; \quad (9)$$

Where $R_{\max}$ is the maximum run length. Eq. (10) – Eq. (16) provide the texture features obtained from the GLRLM. The features used for texture-based evaluation include measurements such as short run emphasize, long run emphasize, and gray level non-uniformity.

(i) Short Run Emphasis (SRE): It is a metric for short run length distribution and higher indicates fine textural textures. It is represented in Eq. (10)

$$SRE = \frac{\sum_{i\in N_g}\sum_{j\in N_r}\frac{Z_{ij}}{j^2}}{\sum_{i\in N_g}\sum_{j\in N_r} Z_{ij}} \quad (10)$$

(ii) Long Run Emphasis (LRE): It is a metric for long run length distribution and higher value indicates coarser structural textures is mentioned in Eq. (11)

$$LRE = \frac{\sum_{i\in N_g}\sum_{j\in N_r} j^2 Z_{ij}}{\sum_{i\in N_g}\sum_{j\in N_r} Z_{ij}} \quad (11)$$

(iii) Gray Level Non-uniformity (GLN): The GLN is a metric used to measure the variation in an image's pixel intensity values, with lower values indicating greater uniformity, indicating less variation in gray levels as in Eq. (12)

$$GLN = \frac{\sum_{i\in N_g}\left(\sum_{j\in N_r} Z_{ij}\right)^2}{\sum_{i\in N_g}\sum_{j\in N_r} Z_{ij}} \quad (12)$$

(iv) Run Length Non-uniformity (RLN): The RLN metric assesses an image's run length consistency, with a lower value indicating greater uniformity and texture homogeneity due to similar run lengths throughout the image. It is mentioned in Eq. (13)

$$RLN = \frac{\sum_{j\in N_r}\left(\sum_{i\in N_g} Z_{ij}\right)^2}{\sum_{i\in N_g}\sum_{j\in N_r} Z_{ij}} \quad (13)$$

(iv) Run Percentage (RP): Proportion of run count to the voxels count in the ROI is used to determine the texture coarseness. The higher values indicate that a large ROI proportion is made up of short runs. It is mentioned in Eq. (14)

$$RP = \frac{\sum_{i\in N_g}\sum_{j\in N_r} z_{ij}}{N} \quad (14)$$

(vi) Low Gray Level Run Emphasis (LGRE): The LGRE metric in Eq. (15) evaluates the presence of lower gray-level values within an image. A higher LGRE value indicates a stronger concentration of low-intensity values, highlighting areas dominated by darker tones.

$$LGRE = \frac{\sum_{i\in N_g}\sum_{j\in N_r} z_{ij}\backslash i^2}{\sum_{i\in N_g}\sum_{j\in N_r} z_{ij}} \quad (15)$$

(vii) High Gray Level Run Emphasis (HGRE): The HGRE metric Eq. (16) assesses the distribution of high-intensity image values. Higher HGRE score indicates a greater concentration of bright or high gray-level areas, signifying regions with stronger intensities.

$$HGRE = \frac{\sum_{i\in N_g}\sum_{j\in N_r} i^2 z_{ij}}{\sum_{i\in N_g}\sum_{j\in N_r} z_{ij}} \quad (16)$$

The GLCM and GLRLM techniques extract feature sets from CT and CXR images, distinguishing textures with similar SRE and LRE values but different gray-level distributions. These handcrafted features are then input into the feature layer (convolutional layer) of RDNN model r for further processing

Deep feature extraction

In order to extract deep features, many layers of convolution, max pooling layers, and FC layers are used. This layered structure enables the model to effectively capture deep features from CT images. The steps involved in this are briefly illustrated below.

Convolution layers

The following is an expression for the convolution layer:

$$h_j^k = b_j^k + \sum w_{i,j}^{k-1} \times x_i^k \quad (17)$$

In Eq. (17) uses the input feature map (x), weight (w), and the bias (b). The output map of features produced by the layer of convolution is denoted by h, the operator × signifies convolution, and k represents the k^{th} convolutional kernel layer.

Max pooling layer

The pooling layer can be described as follows:

$$h_j^{k+1} = f^{max}\left(h_j^k\right) \quad (18)$$

In Eq. (18), f represents the pooling function, specifically the max-pooling operation in this case and h is the output of the layer of pooling.

Fully connected layer

The FC layer receives the hybrid feature vector that has been generated and is shown as:

$$o^l = b^l + w^l h^l \quad (19)$$

Here in Eq. (19), h^l represents the input to the entire connected layer, w^l denotes the weights, and b^l is the bias. o^l stands for the result that corresponds to the deep features that were extracted.

Feature selection

In the feature selection layer, the handcrafted features extracted by image processing techniques like GLCM and GLRLM and deep features extracted from layers of RDNN are concatenated. Then the important feature for classification of diseases are selected by CLM-MWO. The details of feature selection are explained in section 3.

Classification – softmax layer

Finally, the softmax layer is used for categorization process. In the final layer, the softmax function is applied to compute the probability for each image label, as follows:

$$y_j = \frac{e^{o^l}}{\sum_i^{n\_label} e^{o^l}} \quad (20)$$

In Eq. (20), n_label represent numeral quantity of image label, y_j is the estimated label of given test image.

Selecting important feature and optimal parameters of RDNN using CLM-MWO algorithm

The CLM-MWO algorithm is a hybrid approach that combines chaotic theory with MWO to improve feature and parameter selection. It enhances the algorithm's hunting behavior for humpback whales, unlike the original Whale Optimization Algorithm (WOA), which mimics predatory behavior by diving to twelve meters and following a bubble trail to the surface. Here are the steps to follow when participating in the WOA:

Exploitation Phase: During the exploitation phase, the humpback whales target the optimal features and parameters as the optimum prey. They update the position using two strategies like bubble-net feeding and shrinking encircling. Below provided shrink encircling mechanism is utilized for feature selection and parameters optimization.

$$D_f = \left|C \bullet X_f^{\times}(t) - X_f(t)\right| \quad (21)$$

$$X_f(t+1) = X_f^{\times}(t) - A \bullet D \quad (22)$$

$$D_p = \left|C \bullet X_p^{\times}(t) - X_p(t)\right| \quad (23)$$

$$X_p(t+1) = X_p^{\times} - A \bullet D \quad (24)$$

From Eq. (21) – Eq. (24), X_f and X_p represent the whale position for features and parameters selection, while ${X_f}^{\times}$ and ${X_p}^{\times}$ denote the best solution for feature and parameter selection updated during each iteration when a better solution is found. t indicates the current iteration, while D is the distance between the i^{th} whale's position, X and the global best solution, $X^{\times}$. $|\cdot|$ and $\bullet$represents the absolute value operation and element-wise multiplication respectively. In addition, the variables A and C can be found using the following formulas in Eq. (25) and Eq. (26):

$$A = 2a \bullet r - a \quad (25)$$

$$C = 2 \bullet r \quad (26)$$

Where, r represents a randomly generated value within the range of $[0, 1]$ while the parameter a progressively reduces from 2 to 0 throughout the iterative process. The gradual decrease in exploration allows for precise transition from exploration to exploitation for solution refinement. The spiral movement (l) used for adjusting feature and parameter positions is described through a set of Eq. (27) – Eq. (30), which simulate the spiraling path followed by humpback whales when hunting.

$$D'_f = \left|X_f^{\times}\right|(t) - X_f(t) \quad (27)$$

$$X_f(\mathrm{t}+1) = D' \bullet e^{ql} \bullet \cos(2\cos\pi\, l) + X_f^{\times}(t) \quad (28)$$

$$D'_p = \left|X_p^{\times}\right|(t) - X_p(t) \quad (29)$$

$$X_p(\mathrm{t}+1) = D' \bullet e^{bl} \bullet \cos(2\cos\pi\, l) + X_p^{\times}(t) \quad (30)$$

In this case, $D'()$ represents the distance among the solution that has been identified up to that moment and the i^{th} whale. Furthermore, l is a value randomly selected within the interval $[-1, 1]$. The logarithmic spiral shape with q as a constant, is determined by Humpback whales' simultaneous prey capture strategies using a spiral path and shrinking encircling behaviors. To replicate this behavior, 50% probability is applied to feature and parameter selection in equations (31) and (32).

$$X_f(\mathrm{t}+1) = \begin{cases} X_f^{\times}(t) - A \bullet D & if\ r < 0.5 \\ D' \bullet e^{ql} \bullet \cos(2\cos\pi\, l) + X_f^{\times}(t) & if\ r < 0.5 \end{cases} \quad (31)$$

$$X_p(\mathrm{t}+1) = \begin{cases} X_p^{\times}(t) - A \bullet D & if\ r < 0.5 \\ D' \bullet e^{ql} \bullet \cos(2\cos\pi\, l) + X_p^{\times}(t) & if\ r < 0.5 \end{cases} \quad (32)$$

Exploration phase: In this phase, global search mechanism is used to improve the exploration in feature and parameter selection. An arbitrary search agent, instead of the optimal one, guides the search. If $|A| > 1$ or < -1, position updates

follow exploration or exploitation strategies, as defined in Eq. (33) – Eq. (36).

$$D = \left| C \bullet X_{rand} - X_f \right| \quad (33)$$

$$X_f\ (\mathrm{t}+1) = X_{rand} - A \bullet D \quad (34)$$

$$D = \left| C \bullet X_{rand} - X_p \right| \quad (35)$$

$$X_p\ (\mathrm{t}+1) = X_{rand} - A \bullet D \quad (36)$$

In this model, X_{rand} is a randomly chosen as the position vector from the current population. MWO enhances WOA by integrating chaotic techniques to improve convergence speed. Among various chaotic maps utilized for balancing exploration and exploitation, logistic maps significantly boost WOA performance and convergence.

(i) Chaotic Systems: Chaos is a complex system with dependencies on initial conditions and nonlinear irregular waves, enhances global search in optimization by preventing local optima trapping and allowing full exploration using specific range values [18]. The n-dimensional map for feature and parameter optimization is a time-dependent dynamic approach, defined by Eq. (37) and (38).

$$cu_i^{(f+1)} = f\left(cu_i^{(f)}\right) \quad (37)$$

$$cu_i^{(p+1)} = f\left(cu_i^{(p)}\right) \quad (38)$$

A chaotic sequence can be evaluated by initializing the system with an initial state, denoted as $cu_i^{(0)}$. From this starting point, chaotic sequences for feature selection can be defined as $cu_i^{(f)}$, where $f = 0,1,2, \ldots$ and for parameter selection, the sequence is represented as $cu_i^{(p)}$ where $p = 0,1,2, \ldots n$. The study presents a chaotic search algorithm that uses an Ergodic condition to determine the chaotic vector value, employing multiple chaotic functions for various evolutionary paths and utilizing three types of chaotic maps for feature selection and optimization performance.

(ii) Chaotic Maps: A chaotic strategy improves WOA by preventing premature convergence, accelerating optimization, and managing randomness in factor values. Three distinct chaotic maps are employed to enhance feature selection performance, each contributing uniquely to the optimization process, allowing better determination of system states in nonlinear systems.

(A) Logistic map: This map depends on a chaotic system and a nonlinear equation and considered as a second-degree polynomial mapping, utilizing mathematical formulas for feature and parameter selection, as in Eq. (39) and (40):

$$x_f = \mu \times x_{f-1} \times (1 - x_{f-1}) \quad (39)$$

$$x_p = \mu \times x_{p-1} \times (1 - x_{p-1}) \quad (40)$$

The variable μ, which affects the behavior of the system, is usually placed between 0 and 4 in these equations. When $\mu > 4$, the system's values fall outside the interval [0,1]. However, when $\mu = 4$, the system reaches the chaotic state, signifying the onset of chaotic behavior in the mapping process.

(B) Tent map: Within this framework, the parameter μ can only take values between zero and two. At $\mu = 2$, a tent map shows a change from possible stability to disorderly behavior. In order to choose features and parameters, the chaotic map is defined using Eq. (41) and (42):

$$x_f = \begin{cases} \mu \times x_{f-1} & if \quad 0 \le x_f \le 0.5, \\ \mu \times (1 - x_{f-1}) & if\ 0.5 \le x_f \le 1 \end{cases} \quad (41)$$

$$x_p = \begin{cases} \mu \times x_{p-1} & if\ 0 \le x_p \le 0.5, \\ \mu \times (1 - x_{p-1}) & if\ 0.5 \le x_p \le 1 \end{cases} \quad (42)$$

Mathematicians and clinicians have discovered numerous chaotic maps, which are utilized in algorithms to tackle real-world optimization challenges. The fitness function chaotic whale feature selection in Eq. (43) and parameter section Eq. (44)

$$F_f(i) = \max_{\vartheta_f} \left(accuracy\left(X_f\right) - \alpha_f \times \frac{X_f}{n_f} \right) \quad (43)$$

$$F_p(i) = \max_{\vartheta_p} \left(accuracy\left(X_p\right) - \alpha_p \times \frac{X_p}{n_f} \right) \quad (44)$$

Where, $F_f(i)$ and $F_p(i)$ denotes the fitness function for feature and parameter, ϑ_f and ϑ_p represents the whale population for feature and parameter, $accuracy\left(X_f\right), accuracy\left(X_p\right)$ depicts the classification accuracy for feature and parameter selected by whales, α_f and α_p are the weighting parameter, n_f and n_p denotes the total number of features and parameters.

As a result, CLM-MWO-RDNN framework is utilized for effectively classifying Lung disease cases using chest CT images. The trained CT images are processed through a softmax classifier for feature learning and model training. During the validation phase, the framework categorizes images as COVID-19 positive or negative, ensuring an improved convergence rate and more accurate diagnosis.

Algorithm: Proposed CLM-MWO-RDNN model

Input: Training CT images

Output: Final Lung disease detection images

Extract handcrafted features from the training images using GLCM ((Eq. 1) – Eq. (8)) and GLRLM (Eq. (10) - Eq. (16)).

Utilize RDNN's convolutional, max pooling and FC layers to extract deep features.

Select features using the CLM-MWO approach.

Tune parameters of the RDNN model using the CLM-MWO approach.

// *Whale Optimization Algorithm (WOA)*

Set up the whale population at random and the generation counter to g.

Select features ($X_f(i = 1, 2, 3, \dots, n)$) and parameters,$X_p(i = 1, 2, 3, \dots, n)$

Evaluate the fitness of each whale to identify the best whale X^* in the initial population for both feature and parameter

Initialize the chaotic map value x_0 randomly.

While $g <$ greatest number of iteration:

Use the corresponding chaotic maps (the Eq. (41) and Eq. (42)) to update the chaotic map.

for each whale:

Update $a, A, C, l \; and \; r$.

if $\boldsymbol{r < 0.5}$:

if $\boldsymbol{|A| < 1}$:

Apply Eq. (22) and Eq. (24), respectively, to update the whale's position for the feature and parameter.

else if $\boldsymbol{|A| \geq 1}$:

Select a random search whale X_{rand}.

Update the position of current whale using Eq. (34) and Eq. (36).

else if $\boldsymbol{r \geq 0.5}$:

Modify the current whale's position with relation to the feature and parameter.

end for

Check if any whale goes beyond the search space to ensure that each whale is valid.

Compute the fitness of each whale for both feature and parameter as in Eq. (43) and Eq. (44)

Update $X_f^{\times}$ and $X_p^{\times}$ if a better solution is found.

Increment $g = g + 1$.

Return the best feature and parameter sets $X_f^{\times}$ and $X_p^{\times}$.

Train the model with the optimized features and parameters.

Classify test image samples using the trained model and softmax layer (Eq. (20).

Validate the model's performance in classifying Lung Disease cases.

Result and Discussion

Dataset Description

The significance of the suggested model was demonstrated using two separate CT imaging datasets, which are detailed

below.

Dataset 1: Individuals in São Paulo, Brazil, who were actually patients at hospitals, provided the SARS-CoV-2 CT image database [19]. This dataset's principal goal is to support AI research and development efforts aimed at CT scan processing for the detection of SARS-CoV-2 infection. Table 2 details the total number of CT scans used in the performance evaluation from this dataset.

Dataset 2: The Customized Lung Disease collection contains CT pictures of normal, COVID-19, pneumonia, atelectasis, infiltration, and other lung

Table 2. Distribution of CT Images Across Different Disease Categories

Category	Image Count
Normal	1230
COVID	1252
Total	2482

Table 3. CT Image Distribution by Lung Disease Category (Before Augmentation)

Category	Image Count
COVID	1002
Normal	984
Pneumonia	1762
Atelectasis	310
Infiltrate	260
Total	**4318**

Table 4. CT Image Distribution by Lung Disease Category (After Augmentation)

Category	Image Count
COVID	1762
Normal	1762
Pneumonia	1762
Atelectasis	1762
Infiltrate	1762
Total	**8810**

disorders. The images were sourced from public repositories: atelectasis from [20], COVID and Normal from [21], pneumonia from [22] and infiltration from [23]. The total number of CT images for evaluation is shown in Table 3.

Data augmentation is a technique used to artificially improve the size and diversity of a dataset by applying the transformations like rotation, flipping, scaling, zooming and noise addition. In table 2, data augmentation was not applied because the dataset was relatively balanced between COVID and normal cases (1252 vs. 1230), which does not require any augmentation. In contrast, table 3 showed significant class imbalance issues where pneumonia has highest values of 1762 while Infiltrate has 260 values. Hence, it is necessary to upsample the minority classes using data augmentation techniques. Table 4 depicts the after augmentation values equalizing all categories to 1762 images. This ensures that the model treats all classes equally during training, which improves the generalizability and reduces over-fitting.

Experimental Setup and Performance Metrics

This section compares proposed and various lung disease prediction algorithms. Implementation is processed in Matlab 2019b with Windows 10 64-bit machine with an Intel® CoreTM i5-4210 CPU running at 3GHz, 4GB of RAM, and a 1TB hard drive is used. Table 5 depicts the hyperparameter settings of proposed and existing models. For the performance evaluation, the collected dataset is divided into 60% for training i.e., 1489 for dataset 1; 2590 (without augmentation) and 5285 for dataset 2 (with augmentation) and remaining 40% (i.e., 993 for dataset 1; 1728 (without augmentation) and 3525 (with augmentation) for dataset 2, were the test considers the following criteria:

True Positive (TP): Number of lung disease characteristics that were positively confirmed as belonging to the lung diseases.

Table 5. Hyperparameter Settings of Proposed and Existing Models

Ref No.	Hyperparameters	Range
[7]	Learning Rate	0.01
	Optimizer	Stochastic Gradient Descent (SGD)
	Epoch	50
	Batch Size	32
[9]	Learning Rate	0.0001
	Batch size	32
	Epoch	32
	Momentum	0.9
[10]	Optimizer	Adam
	Learning Rate	0.001
	Loss Function	Categorical Cross-Entropy (CE)
	Epochs	60
	Dropout Rate	0.4
[11]	Optimizer	Adam
	Epoch	150
	Batch Size	32
	Learning Rate	0.001
	Momentum	0.9
	Loss Function	CE
[12]	Optimizer	Adam
	Loss Function	CE
[13]	Optimizer	Adam
	Learning Rate	0.001
	Batch Size	32
	Epoch	10

	Loss Function	Binary CE
[14]	Optimizer	Adam
	Learning Rate	0.0001
	Batch Size	32
	Epoch	100
	Loss Function	CE
[15]	Learning Rate	0.01
	Optimizer	Adam
	Epoch	30
Our Work	Learning Rate	0.001
	Weight Decay	0.0005
	Momentum	0.9
	Epoch	250-500
	Batch Size	64
	Loss Function	CE
	Dropout Rate	0.5 -0.2
	Optimizer	CLM-MWO

True Negative (TN): The amount of typical characteristics that were accurately classified as typical.

False Positive (FP): Number of typical characteristics that were wrongly classified as lung disease.

False Negative (FN): Number of COVID-19 or lung disease characteristics that were wrongly classified as normal.

The evaluation measures detailed below are used to assess the efficacy of the suggested approach.

Accuracy: The percentage of right predictions relative to all predictions, as determined by Eq. (45)

$$Accuracy = \frac{TP+TN}{TP+TN+FP+FN} \quad (45)$$

Precision: The percentage of correct predictions relative to a total amount of positive predictions, as determined by Eq. (46).

$$Precision = \frac{TP}{TP+FP} \quad (46)$$

Recall: The percentage of actual positives that are correctly identified, as determined by Eq. (47).

$$Recall = \frac{TN}{TP+FN} \quad (47)$$

F1 Score: The precision and recall harmonic mean, which shows how well they balance each other out, as determined by Eq. (48).

$$F1 - Score = \frac{(2 \times Precision \times Recall)}{(Precision \times Recall)} \quad (48)$$

Receiver Operating Characteristic (ROC) curve: Eq. (49) and Eq. (50) compares the TP rate (TPR) to FP Rate (FPR) for every possible cut-off point of a detection test. The cut of point interval for FPR is fixed between 0.1 to 1. The TPR is found for each interval.

$$TPR = \frac{TP}{TP+FN} \quad (49)$$

$$FPR = \frac{FP}{FP+TN} \quad (50)$$

Performance Analysis

This section assesses and contrasts the suggested CLM-MWO-RDNN model with standard DL models like CNN and CNN-Long Short-Term Memory (LSTM) and Visual Transformer (ViT)-LSTM. CNN, LSTM, ViT and ViT-CNN-LSTM were widely used for image classifcation. CNNs extract features based on spatial relationship among the features, LSTMs capture temporal dependencies and ViTs leverage attention mechanisms for obtaining the global context of images. The proposed CLM-MWO-RDNN model definitely benchmarked if it perform better than those methods. The results proved that proposed work is better than those methods. Table 6 depicts confusion matrix for both dataset usng without augmentation along with single validation and with augmentation along with 4 fold Cross Validation(CV) .

The suggested CLM-MWO-RDNN model is compared to existing models in terms of accuracy, precision, recall and F1-Score in Fig. 2. The results show that the proposed method achieves a higher performance results when compared to other existing models. The accuracy rate of CLM-MWO-RDNN is 14.96%, 11.11%, 8.23% and 3.75% higher than the CNN, CNN-LSTM, ViT-LSTM and ViT-CNN-LSTM models, respectively. The values of proposed other metrics of proposed method also higher than the other DL models.

Table 6. Confusion matrix of two datasets (Test Images)

Datasets	Classes	Confusion Matrix			
		TP	FP	TN	FN
SARS-CoV-2 CT dataset	COVID	490	8	489	6
	Normal	489	6	490	8
SARS-CoV-2 CT dataset with 4 fold CV	COVID	489	13	485	15
	Normal	485	15	477	13
Customised Lung disease dataset (without augmentation and single validation)	COVID	382	20	1307	19
	Normal	383	29	1305	11
	Pneumonia	685	21	1002	20
	Atelectasis	106	23	1581	18
	Infiltrate	98	35	1589	6
Customised Lung disease dataset (with augmentation and 4 fold CV)	COVID	678	26	2794	27
	Normal	680	27	2793	25
	Pneumonia	679	24	2796	26
	Atelectasis	678	25	2795	27
	Infiltrate	680	28	2792	25

Performance Anlaysis for SARS-CoV-2 CT scan dataset (Single validation)

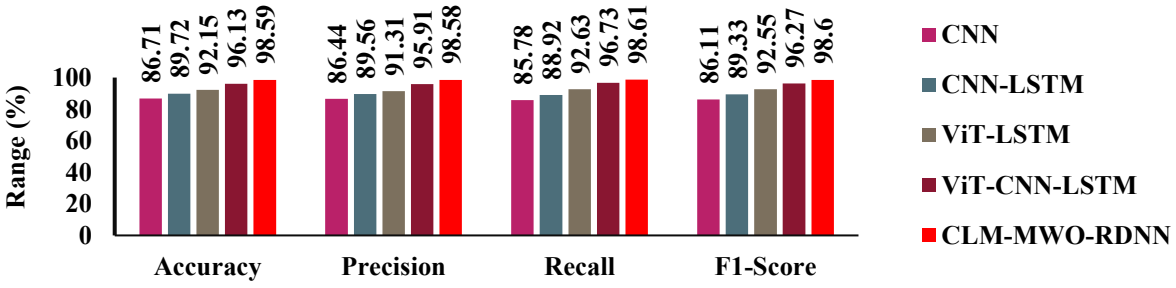

Figure 2. Performance Analysis for SARS-CoV-2 CT scan dataset

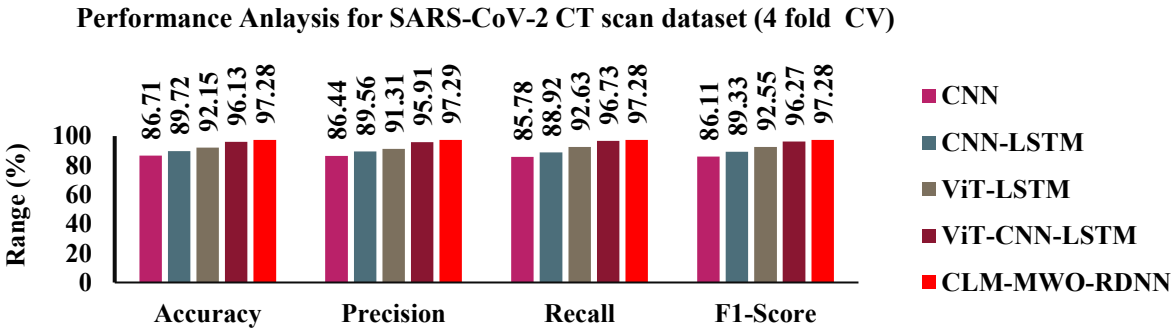

Figure 3. Performance Analysis for SARS-CoV-2 CT scan dataset (4 fold CV)

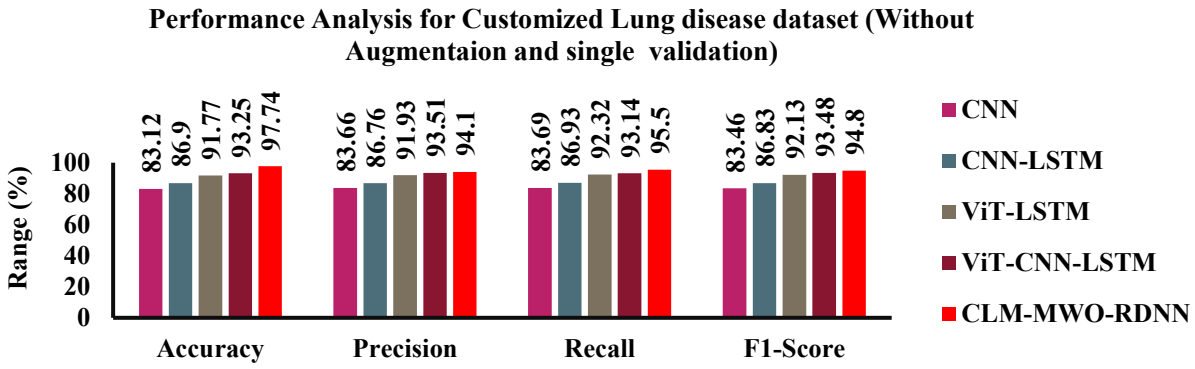

Figure 4. Performance Analysis on Customised Lung disease dataset (without augmentation)

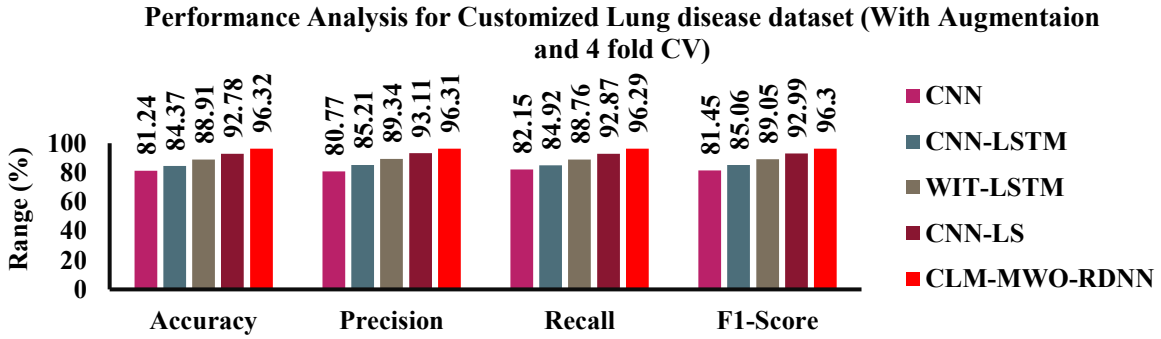

Figure 5. Performance Analysis on Customised Lung disease dataset (with augmentation and 4-fold CV)

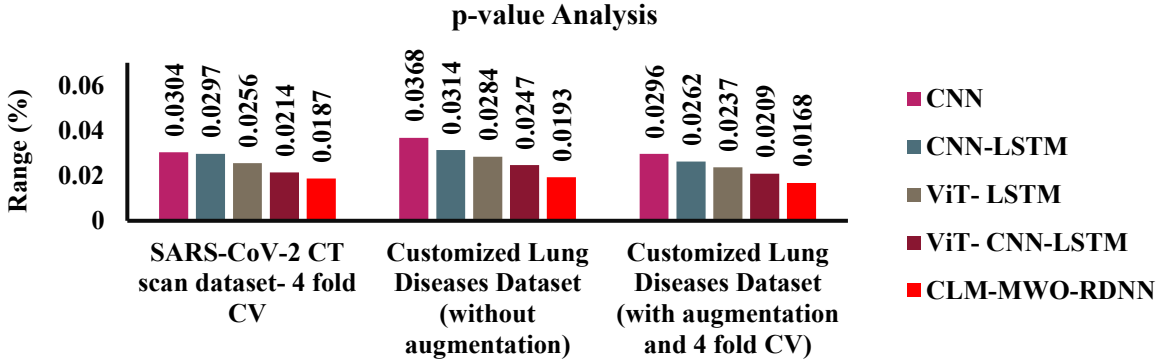

Figure 6. p-value result on Dataset 1 and Dataset 2

The accuracy, precision, recall and F1-Score of the suggested and existing models tested on the customized lung Disease dataset for without augmentation in Fig. 4. In this analysis, CLM-MWO-RDNN model outperforms the other models in terms of accuracy. Fig. 5 shoes the comparison of proposed and existing models on Customised Lung disease dataset (with augmentation and 4-fold cross validation) in terms of accuracy, precision, recall and F1-Score. In this analysis, CLM-MWO-RDNN model outperforms the other models respectively higher than CNN, CNN-LSTM, ViT-LSTM and ViT-CNN-LSTM.

A p-value quantifies the probability of obtaining a particular result if the null hypothesis is true. Fig. 6 provides the comparison of p-values results for proposed and existing models on SARS-CoV-2 and Customised Lung disease dataset (without and with augmentation). In this analysis, the proposed model achieves 0.0187, 0.0193 and 0.0168 $p - value$ on dataset 1 and dataset 2 (without and with augmentation) respectively. This indicates that proposed model has lower p-value that performs better across different datasets resulting in accurate predictions for COVID and other lung illnesses.

Fig. 7 and Fig. 8 present the ROC curves for the proposed CLM-MWO-RDNN model compared to hybrid deep learning models on SARS-CoV-2 and Customised Lung disease dataset (without and with augmentation) respectively. These figures depict the trade-off between TPR and FPR across thresholds, indicating the model's ability to distinguish COVID-19 from non-COVID cases. Curves closer to the top-left corner reflect higher diagnostic accuracy, highlighting the effectiveness of the CLM-MWO-RDNN model in classification.

Table 7 presents the performance analysis of proposed CLM-MWO-RDNN model for handcrafted, deep feature and combined for RDNN model. In this analysis, combined features only achieves 91.45% on SARS-CoV-2 CT, 90.85% (without augmentation) and 88.30% (with augmentation) on customized lung disease datasets. The handcrafted features GLCM and GLRLM provides textural subtleties to RDNN and deep semantic patterns is extracted by RDNN, resulting in better feature representations and accurate Covid-19 diagnosis.

Table 8 presents the performance analysis of proposed CLM-MWO-RDNN model for with and without tuning model hyperparameters on Dataset 1 and Dataset 2. Before hyperparameter tuning, it achieved accuracies of 91.13% on SARS-CoV-2 CT, 90.47% (without augmentation) and 88.74% (with augmentation) on customized lung disease datasets

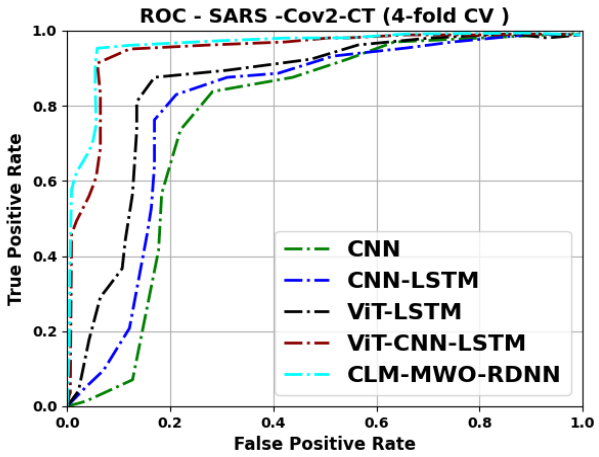

Figure. 7 ROC curve for CLM-MWO-RDNN Model with hybrid DL models on SARS-CoV-2 CT dataset

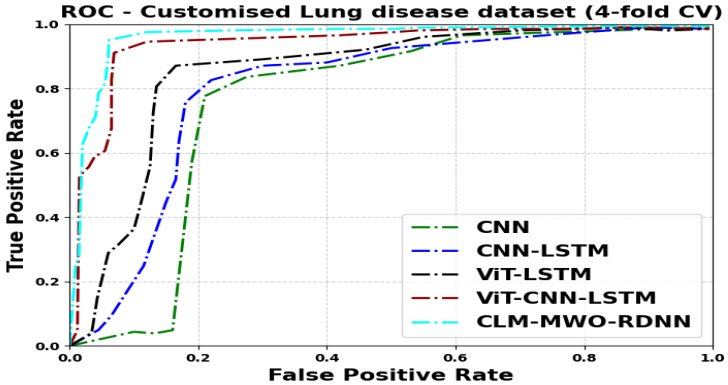

Figure. 8 ROC curve for proposed CLM-MWO-RDNN Model with hybrid DL models for customized lung diseases dataset

Table 7. Comparison of CLM-MWO-RDNN Model performance on various features for Two Dataset

Datasets	Metrics (%)	Test condition		
		RDNN (handcraft feature only)	RDNN model (deep feature only)	Combined handcrafted features with RDNN
SARS-CoV-2 CT	Accuracy	85.61	89.69	98.58
	Precision	84.32	88.97	98.61
	Recall	83.12	89.03	98.55
	F1-score	83.67	89.17	98.57
SARS-CoV-2 CT (4 fold Cross validation)	Accuracy	83..43	86.43	96.98
	Precision	82.56	86.34	96.89
	Recall	81.67	85.85	96.94
	F1-score	81.97	85.23	96.87
Customized Lung Disease CT Images (Without augmentation)	Accuracy	84.34	87.71	97.65
	Precision	85.56	88.47	97.47
	Recall	85.67	87.98	97.72
	F1-score	86.19	88.63	97.61
Customized Lung Disease CT Images (With augmentation and 4 fold CV)	Accuracy	82.56	85.12	95.22
	Precision	83.8	86.11	95.41
	Recall	83.62	85.34	95.35
	F1-score	83.56	85.72	95.50

Table 8. Comparison of RDNN Model for hyperparameter optimization

Datasets	**Metrics (%)**	**Test condition**			
		Without hyperparameter optimization	**Grid search**	**Adam Optimizer**	**Parameter optimization and Feature selection by CLM-MWO)**
SARS-CoV-2 CT	Accuracy	91.13	92.05	92.68	98.59
	Precision	90.91	91.74	92.22	98.58
	Recall	91.63	92.5	93.07	98.61
	F1-score	91.27	92.11	92.64	98.60
SARS-CoV-2 CT(4 fold CV)	Accuracy	91.01	91.88	92.57	97.28
	Precision	90.74	91.45	91.84	97.29
	Recall	91.47	91.98	92.99	97.28
	F1-score	90.99	92.01	92.45	97.28

Customized Lung Disease CT Images (Without augmentation)	Accuracy	90.47	91.38	92.91	97.74
	Precision	91.68	92.30	92.74	94.10
	Recall	90.99	91.92	92.44	95.50
	F1-score	91.28	92.11	92.59	94.80
Customized Lung Disease CT Images (With augmentation and 4 fold CV)	Accuracy	88.74	89.53	90.12	96.32
	Precision	88.12	89.01	90.45	96.31
	Recall	87.79	88.93	90.10	96.29
	F1-score	87.93	88.96	90.26	96.30

Table 9. Computational efficiency of the proposed CLM-MWO-RDNN model using different datasets

Datasets	**Models**	**Training time (sec)**		**Inference time (sec)**		**Memory usage (MB)**	
		CPU	**GPU**	**CPU**	**GPU**	**CPU**	**GPU**
Dataset 1	ViT-CNN-LSTM	4980	1600	440	1300	13800	9400
	CLM-MWO-RDNN	3890	960	240	700	8100	6200
Dataset 1(4 fold Cross validation)	ViT-CNN-LSTM	8520	2360	690	1680	15400	10070
	CLM-MWO-RDNN	7910	1180	380	890	9520	7450
Dataset 2 (Without augmentation)	ViT-CNN-LSTM	9600	3400	750	1800	18600	14000
	CLM-MWO-RDNN	7762	1850	520	1300	16900	12800
Dataset 2 (With augmentation and 4 fold CV)	ViT-CNN-LSTM	10113	3600	790	1950	19100	14700
	CLM-MWO-RDNN	8140	2020	570	1420	17200	13200

Table 10. Comparison of robustness for CLM-MWO-RDNN Model against adversarial noisy mages

Datasets	**Metrics (%)**	**SNR levels in input images**					
		30	**25**	**20**	**15**	**10**	**5**
SARS-CoV-2 CT	Accuracy	67.24	75.76	80.12	85.45	91.91	93.74
	Precision	65.23	74.38	80.56	85.67	92.63	94.12
	Recall	67.14	75.76	80.78	85.34	91.83	93.41
	F1-score	66.54	76.12	81.25	85.49	92.19	94.65
SARS-CoV-2 CT(4 fold Cross validation)	Accuracy	65.13	73.34	76.17	82.34	87.12	91.34
	Precision	65.56	73.76	76.86	82.65	86.54	92.31
	Recall	64.75	72.21	75.34	81.67	85.12	91.32
	F1-score	64.57	72.75	75.12	81.45	86.12	91.12
Customized Lung Disease CT Images	Accuracy	67.32	77.43	82.34	86.12	90.34	93.65
	Precision	68.96	76.98	81.78	86.23	91.92	94.02

(Without augmentation)	Recall	67.67	77.06	82.45	85.98	91.61	93.95
	F1-score	67.45	77.10	83.12	86.38	91.09	93.87
Customized Lung Disease CT Images (With augmentation and 4 fold CV)	Accuracy	65.34	72.89	78.67	83.91	88.73	91.82
	Precision	64.12	71.46	77.45	83.04	88.15	91.23
	Recall	65.87	72.02	78.01	83.56	88.39	91.47
	F1-score	64.99	71.71	77.72	83.29	88.27	91.35

Table 11. Comparison of Different Existing Models and Proposed Model

Ref. No	Models	Dataset	No. of. Images	No. of. class	Training\ Testing\ Validation	Performance Metrics (%)			
						Accuracy	Precision	Recall	F1-Score
[7]	CLM-MWO-INN	SARS-CoV-2 CT scan dataset	2482	2	60\40	91.13	90.91	91.63	91.27
		Lung disease dataset	4318	5	60\40	93.11	85.30	85.92	85.61
[9]	MC-CNN	Radiology Encyclopedia and the Italian Society of Interventional and Medical Radiology (SIRM)	810	3	70\30	98.80	98.60	98.50	-
[10]	Deformable ResNet-50	Images sourced from hospitals in São Paulo, Brazil, and stored in the Kaggle repository.	2481	2	80\10\10	97.6	98.2	96.5	97.3
[11]	COVID-ResNet	SARS-CoV-2 CT scans on Kaggle and COVID-19 on UCSD-AI4H	3227	2	6\2\2	96.89	95.79	98.15	96.96
[12]	DETS-DETSOR	SARS-COV-2 Ct-Scan Dataset	3734	2	70\30	97.2		95.9	
[13]	ConvNeXt	SARS-CoV-2 CT-Scan Dataset	2482		5-fold CV	89.4	87.3	92.9	90
[14]	HTL-FED	300 lung CT scan images from Fariabi Hospital in Kermanshah	3500	2	2,400 (train) 1,500 (test)	97 (Train) 88 (Test)	97 (Train) 88 (Test)	95 (Train) 87 (Test)	-
[15]	VGG-19+ ResNet	CT images collected	2481	2	80\20	98.51	97.47	99.49	-

	50+ RFE	from hospitals across Brazil							
Ours	**CLM-MWO-RDNN**	**SARS-CoV-2 CT scan dataset**	**2482**	**2**	**60\40**	**98.59**	**98.58**	**98.61**	**98.60**
		SARS-CoV-2 CT dataset with 4 fold CV)	**2482**	**2**	**60\40 for each fold**	**97.28**	**97.29**	**97.28**	**97.28**
		Customized Lung disease dataset (without augment)	**4318**	**5**	**60\40**	**97.74**	**94.1**	**95.5**	**94.8**
		Customized Lung disease dataset (with augmentation and 4 fold CV)	**8810**	**5**	**60\40- for each fold**	**96.32**	**96.31**	**96.29**	**96.30**

respectively. After hyperparameter optimization through CLM-MWO, the accuracies improved to 93.69% on SARS-CoV-2 CT, 92.71% (without augmentation) and 91.85% (with augmentation). 93.69% and 92.71%, respectively. Precision, recall, and F1-score also observed significant enhancements across all datasets, indicating that optimal hyper parameters bolstered the model's capacity to accurately predict Covid-19.

Table 9 shows the computational efficiency of the proposed CLM-MWO-RDNN model on SARS-CoV-2 CT and customized lung diseases dataset (without. and with augmentation). The training time, inference time and memory usage are measured separately for CPU and GPU environments The results demonstrate that all the computational efficiency are much faster than other method. Speeds up training and inference while also reducing memory usage. In addition, the scalability is evaluated for SARS-CoV-2 CT and customized lung diseases dataset (without and with augmentation). The analysis states that the dataset size increases, training time increases proportionally with minimal overhead, proving the proposed model is scalable for Covid-19 prediction

Table 10 contrasts the proposed CLM-MWO-RDNN model adversarial noisy images in SARS-CoV-2 CT and customized lung diseases dataset (without and with augmentation). Testing on adversarial images, the proposed model achieves 91.91% on SARS-CoV-2 CT, 90.34% (without augmentation) and (with augmentation) on customized lung diseases dataset correspondingly which reduces its accuracy. Following pre-processing, on both dataset, the accuracy rises to 93.74%, 93.65% and 91.82% respectively. Similar improvements in accuracy, recall and F1-score point to pre-processing greatly improving model performance. This emphasizes the models resilience and the need of data preparation in reducing the influence of the Covid-19 prediction task

Comparative Analysis of state-of-arts models with proposed models

Table 11 displays a comprehensive comparison of the proposed model's results with those of prior research. The existing models referenced in this comparison have been sourced from the literature reviewed in Section 2. In this analysis, Accuracy, precision, recall, and F1-score for CLM-MWO-INN in detecting SARS-CoV-2 were 91.13%, 90.91%, 91.63% and 91.27% respectively. When tested on a lung disease dataset, it achieved 93.11% accuracy, though with slightly lower precision (85.30%), recall (85.92%), and F1-score (85.61%). CLM-MWO-RDNN model, developed in the current study, outperformed all others methods, achieving 98.59% accuracy on SARS-CoV-2 dataset, 97.74% on lung diseases dataset (without augmentation) and 96.32% on lung diseases dataset (with augmentation). Similarly, it demonstrated outstanding precision, recall and F1-scores given in table 10. Overall, CLM-MWO-RDNN model outperformed others models, achieving better outcomes on both datasets.

Potential limitations

The results of the prospeod model can be

affected by Imaging variations like Magnetic Resonance Imaging (MRI) and other medical images. Models perform better on previously observed data. It would be beneficial to have models that can function on data that has never been seen before. The hyper parameter tuning proposed in this study solves these issues significantly. However, transfer learning from pre-

trained models and intelligent data augmentation can further overcome these limitations and approaches.

4. CONCLUSION

This paper proposes the CLM-MWO-RDNN model for Lung disease detection. The main goal of this model is to improve classifier performance by determining the best architecture and informative features. In the RDNN, the CLM-MWO algorithm handles features and parameter selection. In addition, combining deep and handmade features considerably enhances Lung disease identification. The results demonstrate that the suggested method outperforms existing approaches with a superior convergence rate. It obtains an accuracy of 99.69% using the SARS-CoV-2 CT database and 99.71% (without augmentation) and 96.32% (with augmentation) using the customized lung disease dataset. In the future, an advanced model like Generative Adverbial Network (GAN) or improved self-attention mechanism will be developed to address challenges related to performance on unseen data.

REFERENCES

[1] C. Sohrabi, Z. Alsafi, N. O'neill, M. Khan, A. Kerwan, A. Al-Jabir, and R. Agha, "World Health Organization declares global emergency: A review of the 2019 novel coronavirus (COVID-19)", International journal of surgery, Vol.76, pp.71-76, 2020.

[2] Y.C. Liu, R.L. Kuo, and S.R. Shih, "COVID-19: The first documented coronavirus pandemic in history", Biomedical journal, Vol.43, No.4, pp.328-333, 2020.

[3] .L. Sandri, J. Inoue, J. Geiger, J.M. Griesbaum, C. Heinzel, M. Burnet, and A. Kreidenweiss, "Complementary methods for SARS-CoV-2 diagnosis in times of material shortage", Scientific reports, Vol.11, No.1, pp.1-8, 2021.

[4] M. Elsharkawy, A. Sharafeldeen, F. Taher, A. Shalaby, A. Soliman, A. Mahmoud, and A. El-Baz, "Early assessment of lung function in coronavirus patients using invariant markers from chest X-rays images", Scientific Reports, Vol.11, No.1, pp.1-11, 2021.

[5] .H. Kassania, P.H. Kassanib,M.J. Wesolowskic, K.A. Schneidera, and R. Detersa, "Automatic detection of coronavirus disease (COVID-19) in X-ray and CT images: a machine learning based approach", Biocybernetics and Biomedical Engineering, Vol.41, No.3, pp.867-879, 2021.

[6] SA. Bhargava, A. Bansal, and V. Goyal, "Machine learning-based automatic detection of novel coronavirus (COVID-19) disease", Multimedia Tools and Applications, Vol.81, No.10, pp.13731-13750, 2022.

[7] S. Nachimuthu, S. Kaliyamoorthi, "COVID-19 diagnosis using chaotic logistic map based modified whale optimization: A robust feature and parameter selection approach", Revue d'Intelligence Artificielle, Vol. 37, No. 5, pp. 1167-1176, 2023.

[8] I. Chouat, A. Echtioui, R. Khemakhem, W. Zouch, M. Ghorbel, and A.B. Hamida, "COVID-19 detection in CT and CXR images using deep learning models", Biogerontology, Vol. 23, No.1, pp.65-84, 2022.

[9] M.H. Al-Sheikh, O. Al Dandan, A.S. Al-Shamayleh, "Multi-class deep learning architecture for classifying lung diseases from chest X-Ray and CT images", Sci Rep 13, Vol.13, No.1, p.19373 2023.

[10] M. Foysal, A.A. Hossain, A. Yassine, and M.S. Hossain, "Detection of COVID-19 Case from Chest CT Images Using Deformable Deep Convolutional Neural Network", Journal of Healthcare Engineering, Vol. 2023, No.1, p.4301745, 2023.

[11] T. Zhou, X. Chang, Y. Liu, X. Ye, H. Lu, F. Hu "COVID-ResNet: COVID-19 Recognition Based on Improved Attention ResNet", Electronics, Vol.12, No.6, p.1413, 2023.

[12] J.J. Haennah, C.S. Christopher, and G.G. King, "Prediction of the COVID disease using lung CT images by deep learning algorithm: DETS-optimized Resnet 101 classifier", Frontiers in Medicine, Vol.10, p.1157000, 2023.

[13] M. Almutaani, T. Turki, and Y.H. Taguchi, "Novel large empirical study of deep transfer learning for COVID-19 classification based on CT and X-ray images", Scientific Reports, Vol.14, No.1, p.26520, 2024.

[14] H. Salarabadi, M.S. Iraji, M. Salimi, and M. Zoberi, "Improved COVID-19 Diagnosis Using a Hybrid Transfer Learning Model with Fuzzy Edge Detection on CT Scan Images", Advances in Fuzzy Systems, Vol. 2024, No.1, p.3249929, 2024.

[15] M.M. Hossain, M. A.A. Walid, S.S. Galib, M.M. Azad, W.Rahman, A.S.M. Shafi, and M.M.Rahman, "Covid-19 detection from chest ct images using optimized deep features and ensemble classification", Systems and Soft Computing, Vol.6, p.200077, 2024.

[16] Q. Firdaus, R. Sigit, T. Harsono, and A. Anwar, "Lung Cancer Detection Based On CT-Scan Images with Detection Features Using Gray Level Co-Occurrence Matrix (GLCM) and Support Vector Machine (SVM) Methods", In 2020 International Electronics Symposium (IES), pp. 643-648, 2020.

[17] H. Zhang, C.L.Hung, G. Min, J.P. Guo, M. Liu, and X. Hu, "GPU-accelerated GLRLM algorithm for feature

extraction of MRI", Scientific reports, Vol.9,No.1, pp.1-13, 2019.

[18] F.B. Demir, T. Tuncer, and A.F. Kocamaz, "A chaotic optimization method based on logistic-sine map for numerical function optimization", Neural Computing and Applications, Vol. 32, No.17, pp.14227-14239, 2020.

[19] https://www.kaggle.com/plameneduardo/sarscov2-ctscan-datase.

[20] https://radiopaedia.org/articles/lung-atelectasis?lang=us

[21] https://www.kaggle.com/datasets/mehradaria/covid19-lung-ct-scans

[22] https://radiopaedia.org/articles/viral-respiratory-tract-infection.

[23] https://radiopaedia.org/playlists/41156?lang=us.

.